

Two-dimensional Ferroelectric Ferromagnetic Half Semiconductor in VOF monolayer

Shaowen Xu^a, Fanhao Jia^a, Guodong Zhao^{ba}, Wei Wu^a, and Wei Ren^{a†}

^aPhysics Department, Shanghai Key Laboratory of High Temperature Superconductors, State Key Laboratory of Advanced Special Steel, International Centre of Quantum and Molecular Structures, Shanghai University, Shanghai 200444, China.

^bSchool of Microelectronics, Fudan University, Shanghai, China

†renwei@shu.edu.cn

Two-dimensional (2D) multiferroics have been casted great attention owing to their promising prospects for miniaturized electronic and memory devices. Here, we proposed a highly stable 2D multiferroic, VOF monolayer, which is an intrinsic ferromagnetic half semiconductor with large spin polarization $\sim 2 \mu_B/V$ and a significant uniaxial magnetic anisotropy along a -axis ($410 \mu eV/V$ atom). Meanwhile, it shows excellent ferroelectricity with a large spontaneous polarization $32.7 \mu C/cm^2$ and a moderate energy barrier (~ 43 meV/atom) between two ferroelectric states, which can be ascribed to the Jahn-Teller distortion. Moreover, VOF monolayer harbors an ultra-large negative Poisson's ratio in the in-plane direction (~ -0.34). The Curie temperature evaluated from the Monte Carlo simulations based on the Ising model is about 215 K, which can be enhanced room temperature under -4% compressive biaxial strain. The combination of ferromagnetism and ferroelectricity in the VOF monolayer could provide a promising platform for future study of multiferroic effects and next-generation multifunctional nanoelectronic device applications.

Introduction

Two-dimensional (2D) multiferroics represent a class of unique materials¹ with two or more coexisting ferroic orders, such as ferromagnetism/antiferromagnetism, ferroelectricity, and ferroelasticity, which possess promising application prospects in miniaturized information storage and spintronic device²⁻⁹. The microscopic sources of

ferroelectricity lead to two kinds of multiferroics namely type-I and type-II multiferroics¹⁰⁻¹¹. The ferroelectricity and magnetic orderings in Type-I multiferroics have independent origins, which results in a weak magnetoelectric (ME) coupling with high transition temperature and large ferroelectricity polarization, e.g. 2D CuCrP₂S₆¹². In the second group called type-II multiferroics, such as Hf₂VC₂F₂ monolayer¹³ and VS₂ bilayer¹⁴, the ferroelectricity polarization is induced by the magnetic ordering, thereby they often present a strong ME coupling with relatively low transition temperature and weak polarization. Unfortunately, due to the famous d^0 rules¹⁵, most of 2D materials lack intrinsic polarization or ferromagnetic (FM) ordering, which limit their further applications in spintronics. Therefore, pursuing the multiferroic materials simultaneously possessing ferromagnetism and ferroelectricity still remains challenging hitherto¹⁶⁻¹⁷.

Many researches are focused on antiferromagnetic (AFM) and ferroelasticity, for example, AgF₂¹⁸ and VF₄¹⁹ monolayers were proposed to have antiferromagnetic and ferroelastic coexistence; FeOOH monolayer was demonstrated to coexist three ferroics (antiferromagnetic, ferroelastic and ferroelectric) with significant electroelastic and magnetoelastic effects²⁰; FeOX (X= Halogen element)²¹ was found to have high Néel temperatures. All above interesting investigations inspired us to further explore the possibility of coexisting ferromagnetism and ferroelectricity in a single system, e.g., VOF monolayer in this work. Additionally, the auxetic materials have been extensively studied in the past decades, which expand laterally in the elastic range when stretched, while shrink in the transverse direction when compressed. Such negative Poisson's ratio (NPR) effect provides extraordinary mechanical performance and promising applications in electromechanical devices such as biomedicine and sports equipment²²⁻²⁵. However, the available auxetic 2D materials possess a relatively small NPR, for example, black phosphorene is predicted to have NPR -0.027²⁴. Hence, it is highly desired to explore new 2D auxetic materials with large NPRs.

To our knowledge, 2D ferromagnetic ferroelectric multiferroics are still scarce with switchable ferro vectors simultaneously with high Cure Temperature (T_c), large

NPR, and strong anisotropy. Inspired by above mentioned literature, we propose a multiferroic VOF monolayer in this work. First of all, we demonstrate the stability from the dynamic, thermodynamic, and mechanical aspects. We find that the VOF monolayer is an intrinsic ferromagnetic half semiconductor with large spin polarization and strong magnetic anisotropy ($410 \mu\text{eV/V}$). Compared to other 2D auxetic materials, it also possesses a relatively large in-plane NPR (~ -0.34). Additionally, the Curie temperature evaluated from the Monte Carlo simulations based on the Ising model is predicted to be $\sim 215 \text{ K}$, which is close to room temperature when applying -4% biaxial compressive strain. Moreover, it is also demonstrated to be ferroelectric with the polarization $\sim 32.7 \mu\text{C}/\text{cm}^2$. These findings will enrich the family of 2D multiferroics with coexisting ferroelectric and ferromagnetic order, and pave a way for realizing the low dimensional nonvolatile logic and memory devices.

Results and discussion

Structural and Ferroelectric Polarization Properties

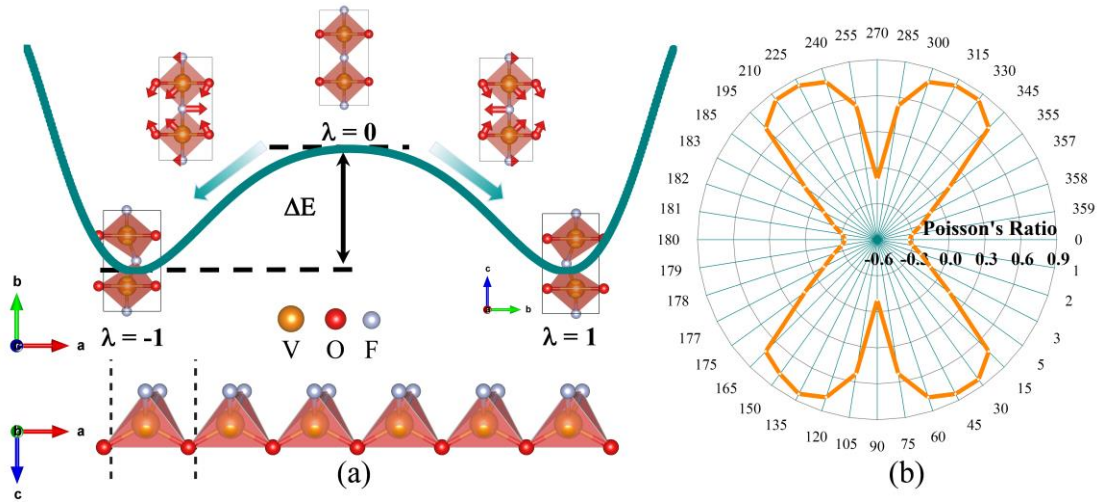


Figure 1. (a) Double well potential of ferroelectric reversal transition in the VOF monolayer, and side views of the VOF monolayer. The rectangles indicate the unit cells. $\lambda=1$, -1 and 0 describe the FE state-1, FE state-2 and centrosymmetric PE phase, respectively. (b) The orientation angle-dependent in-plane Poisson's ratio for VOF monolayer, where the $\theta = 0^\circ$ represents the a -direction.

Bulk VOF is a member of transition metal oxyhalides, which are antiferromagnetic semiconductors with van der Waals (vdW) layered orthorhombic crystal structure (space group 59 $Pmmn$)²⁶⁻²⁷. The monolayer structure taken from the bulk experiences a significant distortion due to the symmetry broken along the c direction, of C_{1h} point group, which is expected to present distinct properties. The top and side views of VOF monolayer are shown in Fig. 1(a).

To verify the stability of the VOF monolayer, we perform the phonon dispersion, molecular dynamic and mechanically simulations. From the perspective of lattice dynamics in Fig.S1(a), we find no appreciable imaginary mode in the phonon dispersion, indicating the dynamitic stability of VOF monolayer. The *ab initio* molecular dynamics (AIMD) simulations at 300 K were performed to check the thermodynamic stabilities as well. We observed in Fig. S1(b), the 2D planar networks and geometry shapes are well preserved, suggesting a robust thermal stability for the VOF monolayer. Moreover, the elastic constants of VOF monolayer meet the Born criteria: $C_{11}>0$, $C_{66}>0$ and $C_{11}*C_{22} > C_{12}^2$, which further confirm that it is mechanically stable.

The optimized structural parameters are displayed in Table I, which shows that the VOF monolayer has the lattice constants of $a = 3.18 \text{ \AA}$, $b = 6.13 \text{ \AA}$, the bond angles $\theta_{O-V-O} = 122.55^\circ$, $\theta_{F-V-F} = 98.67^\circ$ and $\theta_{V-F-V} = 89.65^\circ$. It is easy to see that these systems naturally present an out-of-plane symmetry breaking. It maintains a mirror symmetry plane which is perpendicular to the b -axis, so there is no polarization along the b -axis. Nevertheless, off-center V ions results in the in-plane polarizations along the a -axis in VOF monolayer. To confirm the occurrence of the spontaneous polarization, we adopt an adiabatic pathway from FE phase to PE phase by using an interpolation method. The energies as function of the amplitudes of the in-plane distortions are displayed in the Fig. 1(a), where an interpolation parameter λ is introduced to represent the displacements with respect to the high-symmetry structure. The calculated barrier energy is $\sim 43 \text{ meV/atom}$, which is high enough to ensure the thermal stability of the spontaneous electric polarization at room temperature. Taken the thickness as 5 \AA , the VOF monolayer possesses relatively large in-plane polarization calculated by using

Born effect charge⁷ along the a -axis is $\sim 32.7 \mu\text{C}/\text{cm}^2$, which is comparable and even larger than pervious predicted 2D ferroelectrics, e.g. FeOOH monolayer with the thickness of 6 Å and a polarization $\sim 13 \mu\text{C}/\text{cm}^2$ ²⁰; Taking the thickness as 1 nm, the polarization was reported to be $30.2 \mu\text{C}/\text{cm}^2$ for VOCl₂ monolayer²⁸.

Table I: Structural parameters of VOF monolayer. The lattice constant (Å), bond lengths and bond angles of VOF monolayers by PBE+U.

Lattice Constant (Å)	Bond Lengths (Å)	Bond Angles (°)
a=3.18	2.0 (V-F ₁)	98.67(F-V-F)
b=6.13	2.1 (V-F ₂)	89.65(V-F-V)
	1.86 (V-O)	122.6(V-O-V)

To better understand the origin of ferroelectricity, we plot the d orbital resolved density of states of ferroelectric (FE) and paraelectric (PE) phases calculated by HSE06 functional in Fig.S2. We can easily find the band gap of FE phase is larger than PE phase. For the case of centrosymmetric PE phase, the energy gap between d_{xy} and $d_{xz}+d_{yz}$ orbitals in the proximity of the Fermi level is ~ 0.91 eV. In the FE state, the V ions are displaced along the a -axis, resulting the further splitting of d_{xy} and $d_{xz}+d_{yz}$ orbitals, and widening energy gap (~ 1.11 eV). Consequently, the total energy of the FE state is lower than that of the PE state. The ferroelectric displacement of V atoms could be further understood by the Jahn-Teller distortion mechanism²⁹.

The calculated elastic constants are listed in Table SI. The in-plane Poisson's ratio of orthogonal symmetry monolayers as a function of θ is shown in Fig. 1(b) and calculated by the following equation^{19, 24}:

$$\nu(\theta) = \frac{C_{12} \cos^4 \theta - B \cos^2 \theta \sin^2 \theta + C_{12} \sin^4 \theta}{C_{22} \cos^4 \theta + A \cos^2 \theta \sin^2 \theta + C_{11} \sin^4 \theta} \quad (1)$$

Here, the $A = (C_{11}C_{22} - C_{12}^2)/C_{66} - 2C_{12}$ and $B = C_{11} + C_{22} - (C_{11}C_{22} - C_{12}^2)/C_{66}$, and θ is the angle of the direction with respect to the a -axis. We find that the Young's modulus

for the VOF monolayer varies from 25 N/m to 87 N/m, suggesting the significant mechanical anisotropy of the VOF monolayer. In addition, the in-plane Poisson's ratio presented in Fig.1 (b) exhibits anisotropy along the x (~ -0.34) and y (~ -0.09) directions. Notably, the largest negative and positive Poisson's ratios can reach -0.34 and 0.84 along the x direction and the diagonal direction, respectively. The NPR is much larger than the recently reported 2D auxetic materials, such as δ -phosphorene (-0.267)²⁴ and monolayer black phosphorus with a puckered structure (-0.027)³⁰. In the directions away from x and y axes, VOF monolayer presents a normal positive Poisson's ratio in general.

The Electronic and Ferromagnetic Properties

The band structure and the spin-resolved density of states (DOS) calculated by PBE+ U ($U = 3$ eV) are displayed in Fig.2(a) and Fig.2(b), showing the VOF monolayer is a direct semiconductor with the band gap around ~ 0.42 eV for PBE+ U method (~ 1.7 eV for HSE06 method). The valence band maximum (VBM) and conduction band minimum (CBM) are both located at Γ (0,0) point. Obviously, we can observe the band dispersions along the Γ -X (reciprocal lattice equivalent of the crystallographic a -axis) are steeper than Γ -Y directions near Fermi level, which indicate the electronic anisotropy. From Fig.2(b), we find both the VBM and CBM are predominantly contributed by the V atoms. In more detail, the VBM is majorly originated from V- d_{xy} orbitals with a slight hybridization of O- $2p_y$ states, and the CBM is mainly derived from empty V- d_{xz} orbitals. Remarkably, the VBM and CBM are fully spin-polarized and show the same spin channel, which can be categorised to the class of 2D half semiconductors³¹. A large spin exchange splitting $\Delta = 1.3$ eV is found in the conduction band, making possible to achieve half-metallic characteristic in VOF monolayer. A potential strategy of realizing the half-metal might be applying a negative gate voltage in experiment to inject electrons into the system and produce an electron doping effect³². Hence, we further investigate the carrier-doped electronic properties, demonstrating there exists a semiconductor to half-metal phase transition under carrier doping [see Fig.S3]. In particular, the hole-doped VOF monolayer presents a complete spin-up

polarization, while the electron-doped is first characterized by fully spin-up polarized and then metal properties. Due to the large spin exchange splitting, the half-metallicity can be preserved under a high hole doping density, which is feasible in experiment by using an ionic liquid as a gate dielectric³²⁻³³. All above mentioned results give a potential approach to manipulate the carrier's spin-polarization in VOF monolayer and further simulate the fabrication of the spin-electronic device such as dual-channel field effect spin-filter and spin-valve³⁴.

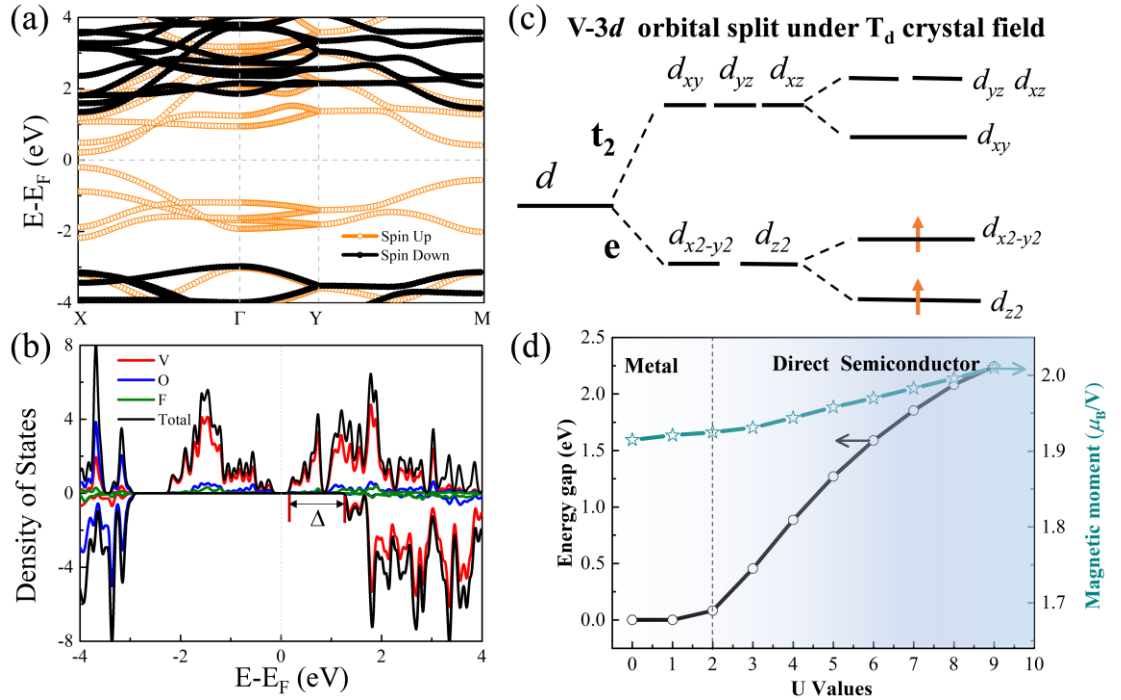


Figure 2. The (a) band structure and (b) partial density of states of VOF monolayer. (c) The schematical illustration of the splitting of the V-3d states under a tetrahedral crystal field. (d) The energy gap and magnetic moment of VOF monolayer as functions of U values.

We determine the magnetic ground state by building 2×1 supercell with four different spin arrangements namely FM, AFM-I, AFM-II and AFM-III, which are illustrated in Fig.S4. The results show that the FM state is the most energetically favourable in all considered structures. The band gaps of VOF monolayer are sensitive to the magnetic ordering, as listed in Table SII. From Fig.S5(a), most of the spin-polarized electrons are located around the V ions, while O atoms carry only tiny local magnetic moments. The magnetic moment is $1.93 \mu_B/V$ atoms, which can be explained

by the electronic configuration of a V atom $[\text{Ar}]3d^34s^2$. Due to the bonding to neighbouring O and F atoms, the V atom loses $3e^-$ and becomes V^{3+} with an electronic configuration of $[\text{Ar}] 3d^2$. According to the Hund's rule, the remaining $2e^-$ on V occupy different d orbitals so that the magnetic moment of V should be $2\mu_B$, close to that obtained from DFT calculations.

Based on the crystal field splitting theory (see Fig.2(c)), we can establish the magnetic exchange paths along the a -axis of V-O-V and V-V chains. The O-mediated super-exchange interaction favors a ferromagnetic coupling between the adjacent V atoms (d_{xy} - $p_{x/y}$ - d_{xy}), while the direct-exchange interaction gives rise to an antiferromagnetic coupling between the adjacent V atoms. According to the Goodenough–Kanamori–Anderson rules³⁵⁻³⁶, FM coupling is favored when the superexchange interaction chains are around 90° , otherwise the AFM coupling is preferred. The bond-angle of V-O-V here (Table I) is close to 90° , which suggests V- d orbitals are nearly orthogonal to the O- p orbitals. We further reveal the real-space wavefunction squared of the highest valence band at the gamma point in the Fig.S5(b), which shows the coexistence V: d_{yz} and O: p_y orbitals and the absence of F orbitals. Therefore, we attribute the stable FM ordering to the competition between the super-exchange and direct-exchange interactions based on the Goodenough-Kanamori-Anderson rules³⁷.

In addition, we checked the effect of Hubbard- U corrections in Fig.2(d). Both electronic and magnetic properties are sensitive to the selected U values. The band gap increases from the value of 0 eV to 2.25 eV (when $U_{\text{eff}} = 9$ eV). The VOF monolayer turns out to be metallic when $U < 2$ eV, while behaves as a semiconductor for larger U over 2 eV, accompanying a metal-insulator transition. It is worth mentioning that different U values do not change the ferromagnetic and ferroelectric ground state, it only modifies the magnetic moment by about $0.1 \mu_B$ from $U=0$ to 9 eV. Thus, we conclude that the basic properties are not altered by the choice of Hubbard U in DFT calculation.

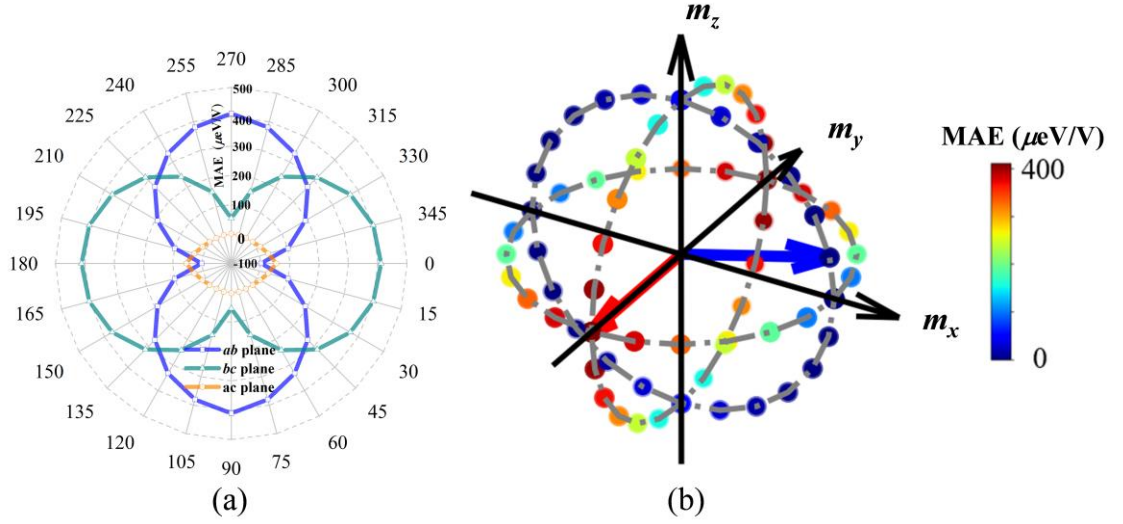


Figure 3. The angular dependence of the MAEs of VOF monolayer with the direction of magnetization lying on three different projected planes (a) and the three-dimensional illustration (b).

Magnetic anisotropy is important to utilize the long-range ferromagnetic ordering³⁸, hence, we consider the spin-orbit coupling (SOC) to evaluate the angle dependent magnetic anisotropy energy (MAE) of VOF monolayer as displayed in Fig.3. It clearly shows that the MAE strongly depends on the direction of magnetization in the *ab* and *bc* planes, while it is much less isotropic in the *ac* plane. The easy magnetization axis is in the *ab* plane and has an angle with *b*- direction of 75° , which makes the VOF monolayer belong to 2D Ising ferromagnetic system³⁹. The MAE reaches a maximum value of $410 \mu\text{eV}$ per V, which is comparable to that of the CrI_3 ($685 \mu\text{eV/Cr}$)⁴⁰, GdI_2 ($553 \mu\text{eV/Gd}$)⁹, and larger than MnAs monolayer ($281 \mu\text{eV/Mn}$)⁴¹ and CrP ($217 \mu\text{eV/Cr}$)⁴².

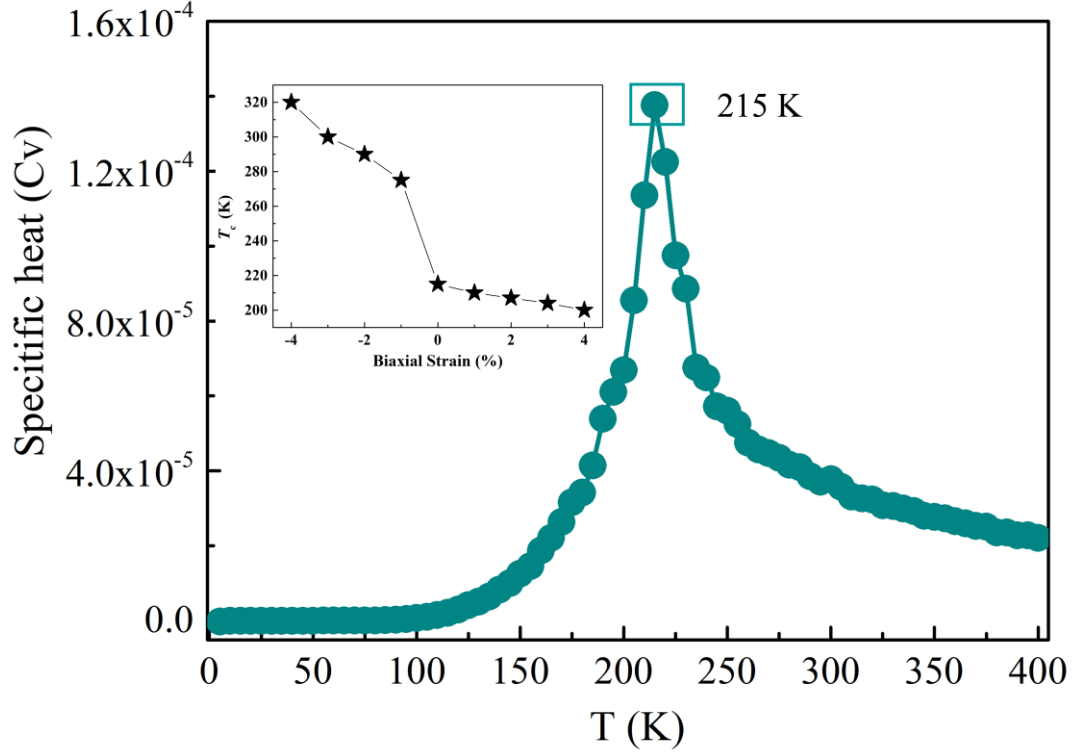


Figure 4. (a) The specific heat capacity (C_v) as a function of temperature for the VOF monolayer. The schematic representation of the exchange interaction is presented in the Figure S4. The inset is the T_c under different biaxial strains of VOF monolayer.

Generally, the Curie temperature T_c is positively correlated with the MAE. We further perform the Monte Carlo (MC) simulations based on the Ising model to estimate the T_c , which was widely used in previous studies. For simplification, we only considered the nearest-neighbor (NN) and next-nearest-neighbor (NNN) exchange interactions. The NN exchange coupling parameters along the a - and b -directions are respectively J_a and J_b , the NNN exchange coupling parameter is J_{ab} , as indicated in the insets of Fig. S3. The Hamiltonian is written as:

$$\mathbf{H} = -2J_a \sum_{\langle ij \rangle} \mathbf{S}_i \cdot \mathbf{S}_j - 2J_b \sum_{\langle\langle ij \rangle\rangle} \mathbf{S}_i \cdot \mathbf{S}_j - 2J_{ab} \sum_{\langle\langle\langle ij \rangle\rangle\rangle} \mathbf{S}_i \cdot \mathbf{S}_j$$

The total energies of four magnetic configurations are expressed below:

$$E_{\text{FM}}/4 = E_0 - 2S^2(J_a + J_b + 2J_{ab}) \quad (2)$$

$$E_{\text{AFM-I}}/4 = E_0 - 2S^2(J_a - J_b - 2J_{ab}) \quad (3)$$

$$E_{\text{AFM-II}}/4 = E_0 - 2S^2(-J_a - J_b + 2J_{ab}) \quad (4)$$

$$E_{\text{AFM-III}}/4 = E_0 - 2S_2(-J_a + J_b - 2J_{ab}) \quad (5)$$

Here, E_0 is the energy of the nonmagnetic part and S is the spin magnetic moment of VOF monolayer. By solving these equations, we obtain the three exchange coupling parameters J_a , J_b and J_{ab} , which are implemented in the MC simulations. We adopt $50 \times 50 \times 1$ square supercell (2500 local magnetic moments) in the simulations. The specific heat C_v as a function of temperature is displayed in Fig.4, which has a peak around $T_c = 215$ K, indicating the ferromagnetic-paramagnetic phase transition. Although the T_c is slightly lower than room temperature, it might be effectively tuned to be close to room temperature by biaxial compressive strains. The T_c of VOF monolayer under different biaxial strain is displayed in the inset of Fig.4. The T_c of the VOF monolayer is enhanced to ~ 320 K by applying -4% biaxial compressive strain, which indicates the intrinsic magnetic field of VOF monolayers is likely to survive at room temperature. We also compared the energy difference between the ferromagnetic and antiferromagnetic states, found that the ferromagnetic is always energetically advantageous under external strains and electric fields, suggesting the FM VOF monolayer is robust against external condition. Furthermore, there are 2D transition metal oxyhalides and nitride monolayers that have been predicted to be ferromagnetic materials with a high Curie temperature, such as CrOCl ⁴³, TcOBr ⁴⁴ and MnNX ($X=\text{F}, \text{Cl}, \text{Br}$ and I)⁴⁵. Another interesting question to consider is about the coupling between ferroelectric and ferromagnetic order. For VOF monolayer system, the easy axis of magnetization is almost perpendicular to the ferroelectric polarization direction, which provides possible direct electric-field control of the magnetization.

Conclusions

In summary, from the first-principles we demonstrate that ferroelectricity and ferromagnetism simultaneously exist in VOF monolayer. The unique crystal structure leads to in-plane spontaneous electric polarization along the a -direction and moderate activation energy barrier. V ions with spin magnetic moment $\sim 2 \mu_B$ are aligned in a ferromagnetic order. The Curie temperature was predicted to be about 215 K from the Monte Carlo simulations based on the Ising model. The easy magnetization axis is

almost perpendicular to the direction of electric polarization. Our findings open a new route for exploring 2D multiferroic materials and building spintronic devices.

Computational Method

The first-principles calculations are carried out within the generalized gradient approximation (GGA) frame proposed by Perdew, Burke, and Ernzerhof (PBE)⁴⁶, which is implemented in the Vienna *ab initio* simulation package (VASP)⁴⁷. We chose the energy cutoff to be 600 eV, and an additional Dudarev's effective Hubbard $U_{\text{eff}} = 3.0$ eV for V-3d orbitals to deal with the self-interaction error⁴⁸. The Γ centered k-grids were adopted to be $6 \times 6 \times 1$. The atomic positions were fully relaxed until the maximal force on each atom was less than 10^{-4} eV/Å. To solve the well-known problem of underestimated band gap of DFT exchange-correlation functionals, the screened hybrid functional HSE06⁴⁹ was applied to calculate the band gaps. We adopted a vacuum layer thicker than 20 Å to avoid the interaction between periodic images. The spin-orbit coupling (SOC) was also considered to take the orientation dependence of spin and orbital magnetic moments into account. The phonon dispersion was calculated by using density-functional perturbation theory as implemented in the PHONOPY package⁵⁰⁻⁵¹, which is also valid in 2D systems^{7, 52}. The calculated polarization values of 2D materials strongly depended on the thickness of slab we chose⁷. In our calculations, we added two additional 1 Å along the *c*-axis on two sides of VOF monolayer for the calculation of volume Ω . The Born effective tensor is defined as: $Z_{i,j}^* = \frac{\Omega}{e} \frac{\partial p_i}{\partial u_j}$, in which e is the charge of electron, p is polarization, and u is the atomic displacement from its high-symmetry nonpolar position.

Conflicts of interest

The authors declare no competing financial interest.

Acknowledgements

This work was supported by the National Natural Science Foundation of China (51861145315, 11929401, 12074241), the Independent Research and Development

Project of State Key Laboratory of Advanced Special Steel, Shanghai Key Laboratory of Advanced Ferrometallurgy, Shanghai University (SKLASS 2020-Z07), the Science and Technology Commission of Shanghai Municipality (19DZ2270200, 19010500500, 20501130600), and High Performance Computing Center, Shanghai University. F.J. is grateful for the support from the China Scholarship Council (CSC).

References

1. Schmid, H., Multi-ferroic magnetoelectrics. *Ferroelectrics* **1994**, *162* (1), 317-338.
2. Seixas, L.; Rodin, A.; Carvalho, A.; Neto, A. C., Multiferroic two-dimensional materials. *Physical review letters* **2016**, *116* (20), 206803.
3. Zhang, S.-H.; Liu, B.-G., A controllable robust multiferroic GaTeCl monolayer with colossal 2D ferroelectricity and desirable multifunctionality. *Nanoscale* **2018**, *10* (13), 5990-5996.
4. Wang, H.; Qian, X., Two-dimensional multiferroics in monolayer group IV monochalcogenides. *2D Materials* **2017**, *4* (1), 015042.
5. Xu, M.; Huang, C.; Li, Y.; Liu, S.; Zhong, X.; Jena, P.; Kan, E.; Wang, Y., Electrical Control of Magnetic Phase Transition in a Type-I Multiferroic Double-Metal Trihalide Monolayer. *Physical Review Letters* **2020**, *124* (6), 067602.
6. Hu, M.; Xu, S.; Liu, C.; Zhao, G.-D.; Yu, J.; Ren, W., First-principles prediction of a room-temperature ferromagnetic and ferroelastic 2D multiferroic MnNX (X= F, Cl, Br, I). *Nanoscale* **2020**.
7. Jia, F.; Xu, S.; Zhao, G.; Liu, C.; Ren, W., Structural and electronic properties of two-dimensional freestanding BaTiO₃/SrTiO₃ heterostructures. *Physical Review B* **2020**, *101* (14), 144106.
8. Tokmachev, A. M.; Averyanov, D. V.; Taldenkov, A. N.; Parfenov, O. E.; Karateev, I. A.; Sokolov, I. S.; Storchak, V. G., Lanthanide f 7 metalloxenes-a class of intrinsic 2D ferromagnets. *Materials Horizons* **2019**, *6* (7), 1488-1496.
9. Wang, B.; Zhang, X.; Zhang, Y.; Yuan, S.; Guo, Y.; Dong, S.; Wang, J., Prediction of a two-dimensional high-TC f-electron ferromagnetic semiconductor. *Materials Horizons* **2020**, *7* (6), 1623-1630.
10. Huang, C.; Du, Y.; Wu, H.; Xiang, H.; Deng, K.; Kan, E., Prediction of Intrinsic Ferromagnetic Ferroelectricity in a Transition-Metal Halide Monolayer. *Physical Review Letters* **2018**, *120* (14), 147601.

11. Khomskii, D., Trend: Classifying multiferroics: Mechanisms and effects. *Physics* **2009**, 2, 20.
12. Lai, Y.; Song, Z.; Wan, Y.; Xue, M.; Wang, C.; Ye, Y.; Dai, L.; Zhang, Z.; Yang, W.; Du, H., Two-dimensional ferromagnetism and driven ferroelectricity in van der Waals CuCrP₂S₆. *Nanoscale* **2019**, 11 (12), 5163-5170.
13. Zhang, J.-J.; Lin, L.; Zhang, Y.; Wu, M.; Yakobson, B. I.; Dong, S., Type-II multiferroic Hf₂VC₂F₂ MXene monolayer with high transition temperature. *Journal of the American Chemical Society* **2018**, 140 (30), 9768-9773.
14. Liu, X.; Pyatakov, A. P.; Ren, W., Magnetoelectric Coupling in Multiferroic Bilayer VS₂. *Physical Review Letters* **2020**, 125 (24), 247601.
15. Huang, B.; Clark, G.; Navarro-Moratalla, E.; Klein, D. R.; Cheng, R.; Seyler, K. L.; Zhong, D.; Schmidgall, E.; McGuire, M. A.; Cobden, D. H., Layer-dependent ferromagnetism in a van der Waals crystal down to the monolayer limit. *Nature* **2017**, 546 (7657), 270-273.
16. Xu, B.; Li, S.; Jiang, K.; Yin, J.; Liu, Z.; Cheng, Y.; Zhong, W., Switching of the magnetic anisotropy via strain in two dimensional multiferroic materials: CrSX (X= Cl, Br, I). *Applied Physics Letters* **2020**, 116 (5), 052403.
17. Guo, Y.; Zhang, Y.; Yuan, S.; Wang, B.; Wang, J., Chromium sulfide halide monolayers: intrinsic ferromagnetic semiconductors with large spin polarization and high carrier mobility. *Nanoscale* **2018**, 10 (37), 18036-18042.
18. Xu, X.; Ma, Y.; Zhang, T.; Lei, C.; Huang, B.; Dai, Y., Prediction of two-dimensional antiferromagnetic ferroelasticity in an AgF₂ monolayer. *Nanoscale Horizons* **2020**, 5 (10), 1386-1393.
19. Zhang, L.; Tang, C.; Du, A., Two-dimensional vanadium tetrafluoride with antiferromagnetic ferroelasticity and bidirectional negative Poisson's ratio. *Journal of Materials Chemistry C* **2020**.
20. Feng, X.; Ma, X.; Sun, L.; Liu, J.; Zhao, M., Tunable ferroelectricity and antiferromagnetism via ferroelastic switching in an FeOOH monolayer. *Journal of Materials Chemistry C* **2020**, 8 (40), 13982-13989.
21. Wang, S.; Wang, J.; Khazaei, M., Discovery of stable and intrinsic antiferromagnetic iron oxyhalide monolayers. *Physical Chemistry Chemical Physics* **2020**, 22 (20), 11731-11739.
22. Liu, B.; Niu, M.; Fu, J.; Xi, Z.; Lei, M.; Quhe, R., Negative Poisson's ratio in puckered two-dimensional materials. *Physical Review Materials* **2019**, 3 (5), 054002.
23. Gao, Z.; Dong, X.; Li, N.; Ren, J., Novel two-dimensional silicon dioxide with in-plane negative Poisson's ratio. *Nano letters* **2017**, 17 (2), 772-777.

24. Wang, H.; Li, X.; Li, P.; Yang, J., δ -Phosphorene: a two dimensional material with a highly negative Poisson's ratio. *Nanoscale* **2017**, 9 (2), 850-855.
25. Mir, M.; Ali, M. N.; Sami, J.; Ansari, U., Review of mechanics and applications of auxetic structures. *Advances in Materials Science and Engineering* **2014**, 2014.
26. Mehdikhani, M., Effects of low and high intensity exercises on serum mean values of myoglobin and heart-type fatty acid-binding protein in athletes. **2010**.
27. Diez, R. P.; Baran, E. J., Structural and vibrational properties of vanadium (III) oxofluoride and oxochloride—a theoretical study. *Journal of Molecular Structure: THEOCHEM* **2005**, 732 (1-3), 155-159.
28. Ai, H.; Song, X.; Qi, S.; Li, W.; Zhao, M., Intrinsic multiferroicity in two-dimensional VOCl_2 monolayers. *Nanoscale* **2019**, 11 (3), 1103-1110.
29. Xu, K.; Xiang, H., Unusual ferroelectricity induced by the Jahn-Teller effect: A case study on lacunar spinel compounds. *Physical Review B* **2015**, 92 (12), 121112.
30. Liu, H.; Neal, A. T.; Zhu, Z.; Luo, Z.; Xu, X.; Tománek, D.; Ye, P. D., Phosphorene: an unexplored 2D semiconductor with a high hole mobility. *ACS nano* **2014**, 8 (4), 4033-4041.
31. Yoo, J.-W.; Chen, C.-Y.; Jang, H. W.; Bark, C. W.; Prigodin, V. N.; Eom, C. B.; Epstein, A. J., Spin injection/detection using an organic-based magnetic semiconductor. *Nature Materials* **2010**, 9 (8), 638-642.
32. Li, X.; Yang, J., CrXTe_3 (X= Si, Ge) nanosheets: two dimensional intrinsic ferromagnetic semiconductors. *Journal of Materials Chemistry C* **2014**, 2 (34), 7071-7076.
33. Yuan, H.; Shimotani, H.; Tsukazaki, A.; Ohtomo, A.; Kawasaki, M.; Iwasa, Y., High-density carrier accumulation in ZnO field-effect transistors gated by electric double layers of ionic liquids. *Advanced Functional Materials* **2009**, 19 (7), 1046-1053.
34. Li, X.; Wu, X.; Yang, J., Half-metallicity in MnPSe_3 exfoliated nanosheet with carrier doping. *Journal of the American Chemical Society* **2014**, 136 (31), 11065-11069.
35. Goodenough, J. B., Theory of the role of covalence in the perovskite-type manganites $[\text{La}, \text{M (II)}] \text{MnO}_3$. *Physical Review* **1955**, 100 (2), 564.
36. Kanamori, J., Crystal distortion in magnetic compounds. *Journal of Applied Physics* **1960**, 31 (5), S14-S23.
37. Kanamori, J., Superexchange interaction and symmetry properties of electron orbitals. *Journal of Physics and Chemistry of Solids* **1959**, 10 (2-3), 87-98.

38. Zhuang, H. L.; Kent, P.; Hennig, R. G., Strong anisotropy and magnetostriction in the two-dimensional Stoner ferromagnet Fe₃GeTe₂. *Physical Review B* **2016**, *93* (13), 134407.
39. Zhao, G.-D.; Liu, X.; Hu, T.; Jia, F.; Cui, Y.; Wu, W.; Whangbo, M.-H.; Ren, W., Difference in magnetic anisotropy of the ferromagnetic monolayers VI₃ and CrI₃. *Physical Review B* **2021**, *103* (1), 014438.
40. Zhuang, H. L.; Xie, Y.; Kent, P.; Ganesh, P., Computational discovery of ferromagnetic semiconducting single-layer CrSnTe₃. *Physical Review B* **2015**, *92* (3), 035407.
41. Wang, B.; Zhang, Y.; Ma, L.; Wu, Q.; Guo, Y.; Zhang, X.; Wang, J., MnX (X= P, As) monolayers: a new type of two-dimensional intrinsic room temperature ferromagnetic half-metallic material with large magnetic anisotropy. *Nanoscale* **2019**, *11* (10), 4204-4209.
42. Ma, A.-N.; Wang, P.-J.; Zhang, C.-W., Intrinsic ferromagnetism with high temperature, strong anisotropy and controllable magnetization in the CrX (X= P, As) monolayer. *Nanoscale* **2020**, *12* (9), 5464-5470.
43. Miao, N.; Xu, B.; Zhu, L.; Zhou, J.; Sun, Z., 2D intrinsic ferromagnets from van der Waals antiferromagnets. *Journal of the American Chemical Society* **2018**, *140* (7), 2417-2420.
44. Pang, Z.-x.; Ji, W.-x.; Zhang, C.-w.; Wang, P.-j.; Li, P., Direction-control of anisotropic electronic properties via ferroelasticity in two-dimensional multiferroic semiconductor XOb₂ (X= Tc, Ru). *Chemical Physics Letters* **763**, 138163.
45. Hu, M.; Xu, S.; Liu, C.; Zhao, G.; Yu, J.; Ren, W., First-principles prediction of a room-temperature ferromagnetic and ferroelastic 2D multiferroic MnNX (X = F, Cl, Br, and I). *Nanoscale* **2020**, *12* (47), 24237-24243.
46. Perdew, J. P., JP Perdew, K. Burke, and M. Ernzerhof, Phys. Rev. Lett. **77**, 3865 (1996). *Phys. Rev. Lett.* **1996**, *77*, 3865.
47. Kresse, G., G. Kresse and J. Furthmüller, Phys. Rev. B **54**, 11169 (1996). *Phys. Rev. B* **1996**, *54*, 11169.
48. Zhang, X.-J.; Liu, B.-G., Strain-driven carrier-type switching of surface two-dimensional electron and hole gases in a KTaO₃ thin film. *Physical Chemistry Chemical Physics* **2018**, *20* (37), 24257-24262.
49. Heyd, J.; Scuseria, G. E.; Ernzerhof, M., Hybrid functionals based on a screened Coulomb potential. *The Journal of Chemical Physics* **2003**, *118* (18), 8207.
50. Togo, A.; Oba, F.; Tanaka, I., First-principles calculations of the ferroelastic transition between rutile-type and CaCl₂-type SiO₂ at high pressures. *Physical Review B* **2008**, *78* (13), 134106.

51. Togo, A.; Tanaka, I., First principles phonon calculations in materials science. *Scripta Materialia* **2015**, *108*, 1-5.

52. Xu, S.; Jia, F.; Hu, S.; Sundaresan, A.; Ter-Oganessian, N. V.; Pyatakov, A. P.; Cheng, J.; Zhang, J.; Cao, S.; Ren, W., Predicting the structural, electronic and magnetic properties of few atomic-layer polar perovskite. *Physical Chemistry Chemical Physics* **2021**, *23* (9), 5578-5582.